REPORT

PLANETARY SCIENCE

Largest recent impact craters on Mars: Orbital imaging and surface seismic co-investigation

L. V. Posiolova[1]*, P. Lognonné[2], W. B. Banerdt[3], J. Clinton[4], G. S. Collins[5], T. Kawamura[2], S. Ceylan[6], I. J. Daubar[7], B. Fernando[8], M. Froment[2,9], D. Giardini[6], M. C. Malin[1], K. Miljković[10], S. C. Stähler[6], Z. Xu[2], M. E. Banks[11], É. Beucler[12], B. A. Cantor[1], C. Charalambous[13], N. Dahmen[6], P. Davis[14], M. Drilleau[15], C. M. Dundas[16], C. Durán[6], F. Euchner[6], R. F. Garcia[15], M. Golombek[3], A. Horleston[17], C. Keegan[1], A. Khan[6,18], D. Kim[6,19], C. Larmat[9], R. Lorenz[20], L. Margerin[21], S. Menina[2], M. Panning[3], C. Pardo[2], C. Perrin[12], W. T. Pike[13], M. Plasman[2], A. Rajšić[10]†, L. Rolland[22], E. Rougier[9], G. Speth[1], A. Spiga[23], A. Stott[15], D. Susko[1], N. A. Teanby[17], A. Valeh[1], A. Werynski[1], N. Wójcicka[5], G. Zenhäusern[6]

Two >130-meter-diameter impact craters formed on Mars during the later half of 2021. These are the two largest fresh impact craters discovered by the Mars Reconnaissance Orbiter since operations started 16 years ago. The impacts created two of the largest seismic events (magnitudes greater than 4) recorded by InSight during its 3-year mission. The combination of orbital imagery and seismic ground motion enables the investigation of subsurface and atmospheric energy partitioning of the impact process on a planet with a thin atmosphere and the first direct test of martian deep-interior seismic models with known event distances. The impact at 35°N excavated blocks of water ice, which is the lowest latitude at which ice has been directly observed on Mars.

Seismic recordings of hypervelocity impacts (>3 km/s) are rare despite being the most common terrain modification process in the Solar System. Earth is shielded by its atmosphere, consequently there are few seismically recorded ground impacts, and meteoroids that do reach the ground usually travel at terminal subsonic velocity and only form small craters (*1*–*3*). The Apollo Passive Seismic Experiments on the Moon recorded ground motions from artificial impacts, but these had slow relative velocities (<2.6 km/s), with respect to typical impact velocities of comets or asteroids colliding with the Moon, and formed craters smaller than 30 m in diameter (*4*). Larger natural impacts on the Moon were detected but have not been associated with imaged craters (*4*, *5*), and all are expected to be smaller than 100 m in diameter (*6*). On Earth, a multitude of seismic events with known source locations, for example, explosion sources, have been used extensively for evaluating seismic velocity models, even down to the Earth's core (*7*). In contrast, there have been only a few confirmed seismic source locations on Mars (all impacts), but these were small (<12 m in diameter) and near InSight (<300 km away), so the seismic paths only sampled the shallow crust (*8*). The two newly formed impact craters reported here allow for an evaluation of deep interior Mars global velocity models and observations of the dynamics of the hypervelocity impact process.

The notable impacts (Fig. 1) were discovered using the Mars Reconnaissance Orbiter (MRO) Context Camera (CTX) (*9*) and the Seismic Experiment for Interior Structure (SEIS) (*10*) of the Interior Exploration using Seismic Investigations, Geodesy and Heat Transport (InSight) mission (*11*). Our CTX team independently discovered the Amazonis crater that we associated with the S1094b event. The earlier S1000a event, given its similar seismic signature, was then used to direct a search with MRO cameras to find the Tempe impact crater site. Both impacts generated craters >130 m in diameter, making them the largest fresh craters identified since the beginning of the MRO mission 16 years ago. The seismic events have identifiable surface waves, distinguishing them from other recorded and analyzed events on Mars and indicating shallow sources (*12*). Before these events, surface waves had not been unambiguously identified on any terrestrial planet other than Earth. The closer impact (S1094b) occurred at a distance of 58.5° (3460 km) from the InSight lander on 24 December 2021 and formed the larger of the two craters (150 ± 10 m in diameter). The other impact (S1000a) occurred at a distance of 126° (7455 km) from the InSight lander on 18 September 2021 and formed a cluster of craters (the largest being 130 ± 12 m in diameter). The formation of the craters was time-constrained using the MRO Mars Color Imager (MARCI) (*13*) to within a day (table S1), making the association with the seismic events highly probable. The seismic events associated with the impacts have similar characteristics, both with ~4.0 magnitudes (tables S1 and S2). Because the seismic waves traveled deep in the mantle, both events are critical for analysis of mantle velocity models. However, given the S1000a event's long distance from the lander, direct seismic waves are eclipsed by Mars' core (*14*) and more-complex bouncing seismic body wave phases (*PP* and *SS*) were detected (fig. S1). The additional attenuation and scattering experienced by these waves obscure the source characteristics, making source analysis much more challenging. In addition, the S1000a-associated crater is located on the side of a graben (fig. S2), which perturbed the blast pattern and prevented an easy identification of impactor parameters. In contrast, the closer impact (S1094b) occurred in a flat, dust-covered region. We first analyze the impact process for this closer impact before considering the implications for Mars interior models of both impacts.

Prominent surface albedo disturbances surrounding the S1094b impact allow for the estimation of ephemeral events that would otherwise be unknown, such as the impactor trajectory and the extent of atmospheric blast waves (Fig. 2 and fig. S3). The bearing of the bolide was estimated to be 60° ± 5° clockwise from north by measuring the up-range "forbidden zone" (*15*) in the albedo ray pattern and a down-range extended cluster of secondary impacts. We infer that the impactor approached the surface at an elevation angle of ~30° from horizontal. A steeper angle requires the asymmetric ejecta pattern to be muted, and a much

[1]Malin Space Science Systems, San Diego, CA, USA. [2]Université Paris Cité, Institut de Physique du Globe de Paris, CNRS, Paris, France. [3]Jet Propulsion Laboratory, California Institute of Technology, Pasadena, CA, USA. [4]Swiss Seismological Service, ETH Zurich, Zurich, Switzerland. [5]Department of Earth Science and Engineering, Imperial College London, London, UK. [6]Institute of Geophysics, ETH Zurich, Zurich, Switzerland. [7]Department of Earth, Environmental, and Planetary Sciences, Brown University, Providence, RI, USA. [8]Department of Earth Sciences, University of Oxford, Oxford, UK. [9]Earth and Environmental Sciences Division, Los Alamos National Laboratory, Los Alamos, NM, USA. [10]Space Science and Technology Centre, School of Earth and Planetary Sciences, Curtin University, Perth, WA, Australia. [11]NASA Goddard Space Flight Center, Greenbelt, MD, USA. [12]Nantes Université, Université Angers, Le Mans Université, CNRS, UMR 6112, Laboratoire de Planétologie et Géosciences, Nantes, France. [13]Department of Electrical and Electronic Engineering, Imperial College London, London, UK. [14]Department of Earth, Planetary, and Space Sciences, University of California, Los Angeles, CA, USA. [15]Institut Supérieur de l'Aéronautique et de l'Espace ISAE-SUPAERO, Toulouse, France. [16]U.S. Geological Survey, Astrogeology Science Center, Flagstaff, AZ, USA. [17]School of Earth Sciences, University of Bristol, Bristol, UK. [18]Physik-Institut, University of Zurich, Zurich, Switzerland. [19]Department of Geology, University of Maryland, College Park, MD, USA. [20]Johns Hopkins Applied Physics Laboratory, Laurel, MD, USA. [21]Institut de Recherche en Astrophysique et Planétologie, Université Toulouse III Paul Sabatier, CNRS, CNES, Toulouse, France. [22]Université Côte d'Azur, Observatoire de la Côte d'Azur, CNRS, IRD, Géoazur, Valbonne, France. [23]Laboratoire de Météorologie Dynamique/IPSL, Sorbonne Université, CNRS, Ecole Normale Supérieure, PSL Research University, Ecole Polytechnique, Paris, France.
***Corresponding author. Email: posiolov@msss.com**
†Present address: Department of Earth, Atmospheric, and Planetary Sciences, Purdue University, West Lafayette, IN, USA.

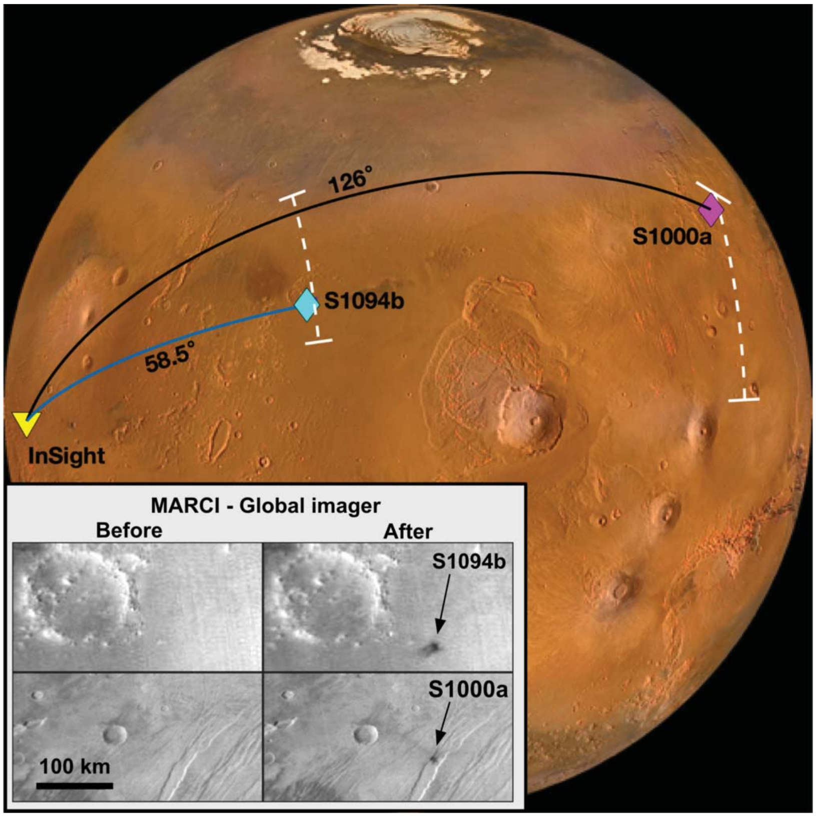

Fig. 1. Impact event location map. The location of the impact craters (diamonds) and the InSight lander (yellow triangle) are shown. The S1094b crater is located at 34.80°N, 189.92°E in Amazonis Planitia. The S1000a crater is located at 38.11°N, 280.12°E in Tempe Terra. The great-circle paths between the new craters and InSight are superimposed onto the underlying globe image derived from MARCI (*13*), Mars Orbiter Camera (*49*), and Mars Orbiter Laser Altimeter (MOLA) data (*50*). The seismic epicentral distance estimates are indicated by the dashed white lines that extend over the azimuthal uncertainty estimate. The inset shows MARCI images from before and after the impacts. The MARCI images have ~2 km per pixel resolution at nadir.

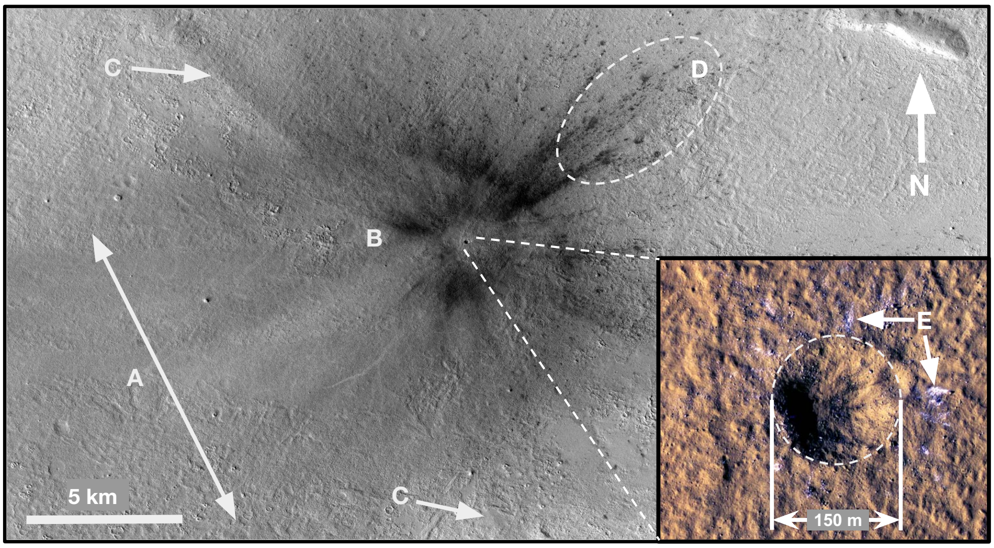

Fig. 2. Orbital images of the impact crater and surrounding area. CTX image (main panel; image ID U05_073077_2154_XI_35N170W): The hypervelocity impactor traveled from southwest to northeast at an inferred azimuth of ~60° (fig. S3), creating a Mach cone shock wave that altered the surface albedo up-range of the impact, region labeled A in the figure. The inner dark ring, near B, is interpreted to be the result of blast wave mobilization of surface fines, impact-derived material directly deposited on the surface, or by ejecta-induced disturbances of the surface dust. The absence of up-range ejecta disturbances indicates an oblique (~30° elevation) impact (*15*). Faint arcuate rays, labeled C, emanating cross-track of the impactor were likely caused by the superposition of the Mach cone and the atmospheric blast (*17*), indicating that both blast waves propagated out at least 18 km. The long-range ejecta–induced disturbances are concentrated in the down-range direction, region D, extending to at least 37 km. HiRISE image (inset; image ID ESP_073077_2155): The crater has a rim-to-rim diameter of ~150 m. The crater floor has an irregular shape, with a depth of roughly 21 m. The light-toned material, for example, areas indicated by arrows labeled E, around the crater is inferred to be water ice ejected during the impact.

CREDIT: (CTX IMAGE) NASA/JPL-CALTECH/MSSS; (HIRISE IMAGE) NASA/JPL-CALTECH/UNIVERSITY OF ARIZONA

shallower angle should have led to an elliptical crater planform (*15*, *16*). Two distinct arcuate rays ("scimitars") extending approximately northwest and south of the impact site likely formed from the superposition of two atmospheric blast waves disturbing surface dust: one generated by the passage of the meteoroid through the atmosphere (Mach cone) and the other by the ground impact (*17*), thus indicating that both blast waves extended to at least 18 km laterally. These arcuate rays provide an independent, albeit consistent, measure of the impactor trajectory (56°). The meteoroid struck the surface at 18:49 LMST (Local mean solar time, thus impacting on the orbital trailing side of Mars. We estimate the radial extent of surface dust disturbance from the crater to be 9 km (fig. S3). This limit is consistent with the

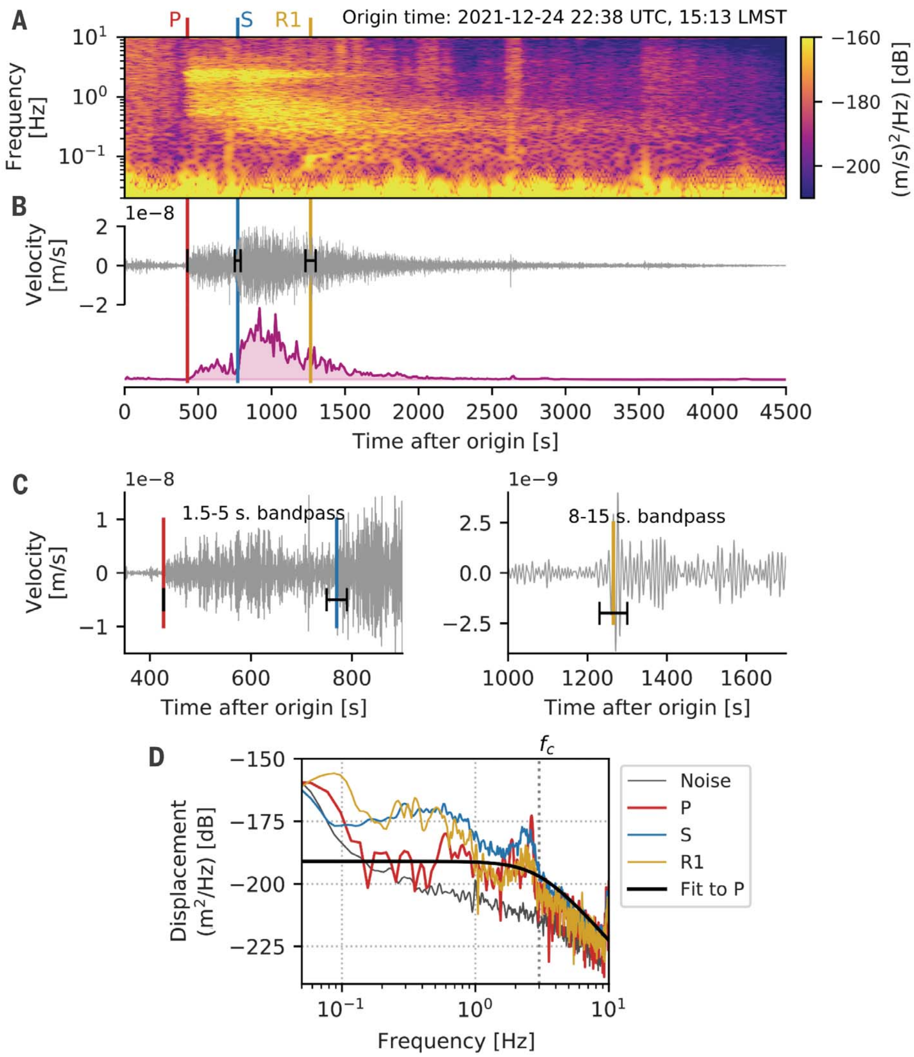

Fig. 3. Seismic observation of S1094b, using de-glitched broadband data. (**A**) Vertical component velocity spectrogram. The event occurred at the end of a noisy period typical of martian afternoons. (**B**) Vertical component velocity time series bandpassed between 1 and 10 s and the derived spectral envelope. Phase picks for *P*, *S*, and Rayleigh (R1) wave arrivals are indicated with pick uncertainty indicated by black bars in the time series. (**C**) Waveform details of the *P* and *S* body waves (left) and Rayleigh wave (right). (**D**) Displacement spectra for the *P*, *S*, and Rayleigh waves and pre-event noise. See fig. S1 for a similar analysis of S1000a.

atmospheric blast pressure produced by a 0.1 to 1 kiloton (4×10^{11} to 4×10^{12} J) surface explosive source (fig. S4). The size of the atmospheric blast allows us to evaluate its contribution to the seismic signal.

Crater size is an important quantity for estimating the kinetic energy and momentum of the impactor for use in numerical models. An image from another camera on MRO, the High Resolution Imaging Science Experiment (HiRISE) (*18*), revealed additional details of the crater and its immediate surroundings (Fig. 2). The crater is irregular in shape, with an estimated rim-to-rim diameter of 150 ± 10 m. Its depth, measured from crater floor to crater rim on the basis of photogrammetry results using HiRISE stereo images, is roughly 21 m. The abundant craters surrounding this impact are likely almost all secondaries generated by the primary impactor, as, in comparison, areas far (>10 to 20 km) from the new impact have few small craters. The bright patches and blocks surrounding the crater reveal that it excavated water ice from the subsurface at a lower latitude (35°N) than any prior ice-exposing crater (39°N) (*19*).

The geological context from orbital imagery aids in determining the appropriate physical models to use in numerical calculations. The S1094b crater is in the Amazonis Planitia region in an area of rugged volcanic plains (*20*), with CTX images showing lava-flow morphologies mantled by a modest cover of debris. The lava flow indicates that a target ground with properties of porous fractured basalt is appropriate for modeling the surface impact. To account for a harder rock site at the crater compared with the region around InSight, we use a local subsurface velocity model based on terrestrial lava flows (*21*) extrapolated to Mars surface conditions (*22*, *23*) (figs. S5 and S6) for seismic modeling.

The seismic source duration for an impact of this size is expected to be shorter than the crater formation time scale and limited to the duration of the nonlinear shock wave propagation regime (*6*). The seismic event S1094b had a very broad frequency content and relatively flat spectra, from 0.1 Hz to 3 Hz (Fig. 3), with a signal lasting >100 min (*24*) owing to propagation coda (*25*). The event had an impulsive first-arrival *P* wave (1-s uncertainty), followed by an emergent strong *S* wave 6 min later (20-s uncertainty). The third wave observed, arriving 8 min later, was a Rayleigh surface wave, expressed as a long-period dispersed pulse with an 8- to 15-s period (*12*). All body wave phases are characterized by a long coda, indicative of strong scattering due to a near-surface source. The spectra display unusually high corner frequencies (3 Hz) compared with most other seismic events recorded on Mars. Shock physics modeling of the impact in a porous fractured basalt target (Fig. 4) indicates that most of the seismic moment was contained within a few hundred meters of the impact (Fig. 4A, orange bar). The moment release occurred over a short time period consistent with the cutoff frequency of 3 Hz identified in the *P*-wave displacement spectrum (Fig. 3D). Above the cutoff frequency, the amplitude shows a cubed frequency drop-off, as also observed for closer, smaller impacts on Mars (*8*) and for shallow explosions on Earth (*26*, *27*).

Seismic moment (M_0) is the key quantity that links the orbital observations of the impact and the impactor parameters to the seismic observations. For S1094b, the seismic moment estimate from *S* body waves was originally calculated assuming a marsquake at 50 ± 30 km depth to be 1.3×10^{15} N·m (*28*). However, the impact seismic source deposits its energy at much shallower depths, in the strongly shocked region, estimated by impact modeling to be at a depth of between 17 and 120 m, or ~50 m (Fig. 4B). We use our lava-flow seismic velocity model to conclude that the moment of a source at this depth is ~100 times smaller than a corresponding deep-crustal source for the same observed amplitude (Fig. 4A and fig. S5). This is comparable to the seismic moment estimated from surface wave spectra, $M_0 = 7.5 \times 10^{13}$ N·m, at the same source depth (fig. S7).

Empirical and numerical models were used to compute seismic moments for S1094b on

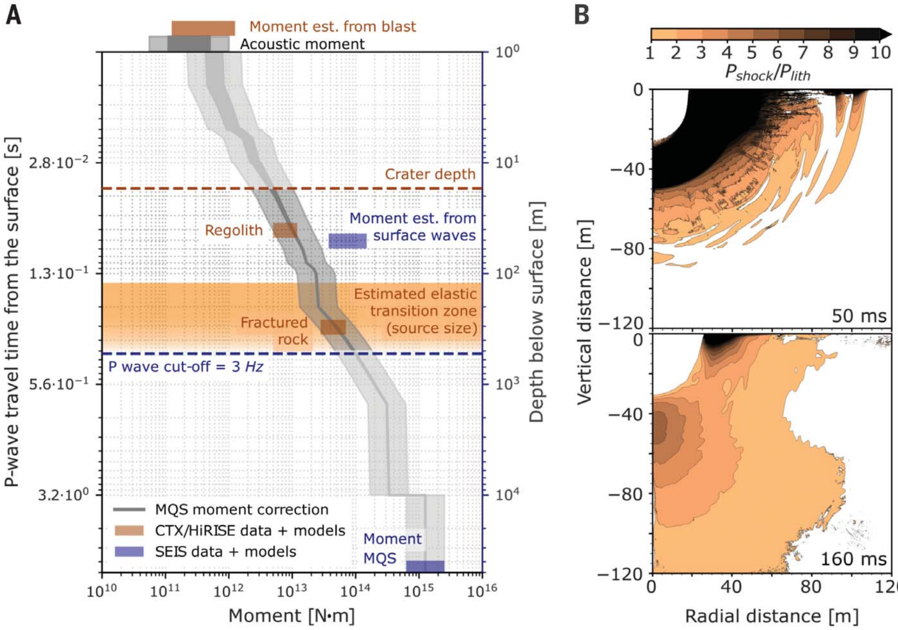

Fig. 4. Seismic source analysis for impact S1094b. (**A**) Seismic moment extrapolated to different source depths and in the air (gray). The blue bars are MQS moment and moment from surface wave amplitude. For more details on the moment/depth relation and modeling methodology see figs. S5 and S6. The brown bars show three moment calculations: two seismic moments estimated from crater size assuming different target materials (*29*, *30*) and one acoustic moment at the surface. Note the overlap between the predicted moment from the atmospheric blast and the estimated acoustic moment (brown and gray bars, respectively). The orange-shaded region indicates the estimated depth range for the transition from shock to elastic waves (*29*). (**B**) iSALE-2D hydrocode simulation of shock wave caused by a vertical impact at 12 km/s of a 5-m-diameter (180 ton) meteoroid into fractured basalt. Two snapshots, at 50 and 160 ms, show the zone of seismic wave generation where the shock pressure (P_{shock}) is substantially higher than the lithostatic pressure (P_{lith}).

the basis of the observed crater size. The imaged crater diameter of 150 ± 10 m corresponds to a vertical impactor momentum of $3.3 \pm 1.4 \times 10^9$ N·s according to empirical crater-scaling relationships and impactor mass, angle, and velocity probability distributions (figs. S8 and S9). For these values, numerical simulations predict seismic moments of 0.5×10^{13} to 1.2×10^{13} N·m for impacts in regolith and 2.8×10^{13} to 7×10^{13} N·m for fractured rock conditions (*29*, *30*). These estimates are consistent with the observed seismic moment corrected for relevant depths in our subsurface model (Fig. 4A). The seismic efficiency was estimated to be 10^{-5} on the basis of scaling relations between seismic moment and crater diameter (*31*) with an order of magnitude uncertainty. This is lower than values estimated for lunar and Earth analogs (*32*) but larger than that previously modeled for small martian impact craters (*29*).

The extensive blast pattern around the S1094b crater suggests that some of the seismic energy may have also originated from energy released in the atmosphere and then coupled to the ground. Numerical impact simulations suggest that up to 10% of the impact energy was partitioned into kinetic energy on the planetary surface, primarily in the ejecta (*33*). For impact scenarios on Mars similar to S1094b, simulations with an atmosphere further suggest that ~5% of the impact energy is partitioned into the blast wave (*34*). An estimated impact energy of between 1×10^{13} and 8×10^{13} J (fig. S4) could produce an atmospheric blast comparable to a 0.1 to 1 kiloton (4×10^{11} to 4×10^{12} J) surface explosion. Therefore, both seismic and image observations are consistent with such a blast and provide coherent constraints in time and space, respectively. Semiempirical airblast theory (*35*) extrapolated to Mars suggests that such a blast would transition from the strong shock regime after 0.2 to 0.4 s, which is consistent with the observed ~3 Hz *P*-wave cut-off frequency. The induced blast pressure is sufficient to mobilize surface dust to a radius of ~10 km, which is consistent with the observed disturbed dust pattern (Fig. 1 and figs. S3 and S4). The estimated blast energy translates to an atmospheric moment $M_0 \approx (\gamma - 1)E = 0.1 \times 10^{12}$ to 1.3×10^{12} N·m, where γ is the adiabatic index (1.33 for Mars), and E is the blast energy (*36*). This is remarkably consistent with the moment-depth model when extrapolated to the surface (Fig. 4A), implying that a moment of only 10^{12} N·m released in the atmosphere could explain a substantial part of the seismic body wave signal, with the remaining part coming from direct coupling of the impactor with the ground.

On Earth, atmospheric explosions easily excite surface waves (*37*) and are highly sensitive to burst altitude (*38*). Solid Mars Rayleigh modes with atmospheric coupling (*14*, *39*) are predicted to have excitation coefficients up to 10 times larger for a near-surface atmospheric source compared with one that is 50 m below the subsurface (fig. S7). Surface waves are expected to have an increase in the excitation coefficients between 0.1 and 0.15 Hz for sources above 50 m altitude. The increase is not observed in the estimated S1094b spectra and may be due to attenuation and scattering, which is not unexpected given that scattering effects are predicted to generate increasing attenuation of surface waves with frequency on the Moon and Mars (*40*). Comparison of S1094b surface wave spectra with near-surface excitation coefficients (fig. S7) suggests that a portion of the surface wave signal could have originated from the blast just above the surface.

The Marsquake Service (MQS) (*41*) using SEIS data (*24*) estimated the seismic locations for both events (S1094b and S1000a). The distance to the events is determined using *S*-minus-*P* arrival times (*SS*-minus-*PP* for S1000a) (*42*, *43*) and polarization measurements of *P* and Rayleigh waves (*PP* for S1000a) (*12*). For the closer event, S1094b, the epicentral distance from the InSight lander was estimated to be 59.7° ± 6.1° (3530 ± 360 km), as compared with the actual distance of 58.5° (3460 km), a difference of only 70 km. For the second impact S1000a, the distance was estimated at 128.3° ± 19° (7591 ± 1240 km), as compared with the actual distance of 126.1°, a difference of 130 km. Additional source parameters for these events are detailed in tables S1 and S2.

The close agreement between distance estimates and the imaged locations increases our confidence in the martian seismic velocity models (*44*–*48*) for the regions sampled by the direct body waves (fig. S10). In particular, the models indicate the absence of mantle discontinuities in the 600 to 700 km depth range, which is the depth at which the *P*, *S*, *PP*, and *SS* waves turn (*44*). For the S1000a event, the P_{diff} phase, the *P* wave that diffracts along the core mantle boundary (CMB), has been tentatively identified (*14*). The PP-P_{diff} travel time difference is sensitive to lower mantle *P* velocities below 800 km. Current models at these depths are constrained by core-reflected *S* phases and the mineral physics–based V_P/V_S ratio (fig. S10). The observed PP-P_{diff} does not match the predicted values given by these models. This mismatch implies that either the *P* velocities at the CMB need adjustment, or the V_P/V_S ratio in the lower mantle is different from current predictions. These two events act as calibrated measurements and help select among various martian interior seismic velocity models (*44–48*); they corroborate Mars mantle velocity models to 800 km depth and will help to improve future models down to the CMB.

The first two recorded teleseismic events on Mars with orbital ground-truth observations have been used to constrain martian interior seismic velocity models and infer dynamic impact processes including seismic moment release, impact source duration, and atmosphere-subsurface energy partitioning. The success in observing the formation of impact craters on Mars using instruments on several missions opens up a more detailed understanding of impact dynamics, atmospheric physics, and the exploration of planetary interiors.

REFERENCES AND NOTES

1. W. N. Edwards, D. W. Eaton, P. G. Brown, *Rev. Geophys.* **46**, RG4007 (2008).
2. P. Brown *et al*., *J. Geophys. Res. Planets* **113**, E09007 (2008).
3. E. Gnos *et al*., *Meteorit. Planet. Sci.* **48**, 2000–2014 (2013).
4. Y. Nakamura, G. V. Latham, H. J. Dorman, *J. Geophys. Res.* **87**, A117–A123 (1982).
5. P. Lognonné, C. L. Johnson, in vol. 10 of *Treatise on Geophysics: Second Edition*, G. Schubert, Ed. (Elsevier, 2015), pp. 65–120.
6. T. V. Gudkova, Ph. Lognonné, J. Gagnepain-Beyneix, *Icarus* **211**, 1049–1065 (2011).
7. W. Wang, J. E. Vidale, *Sci. Adv.* **8**, eabm9916 (2022).
8. R. F. Garcia *et al*., *Nat. Geosci.* (2022).
9. M. C. Malin *et al*., *J. Geophys. Res. Planets* **112**, E05S04 (2007).
10. P. Lognonné *et al*., *Space Sci. Rev.* **215**, 12 (2019).
11. W. B. Banerdt *et al*., *Nat. Geosci.* **13**, 183–189 (2020).
12. D. Kim *et al*., *Science* **378**, 417–421 (2022).
13. J. F. Bell *et al*., *J. Geophys. Res. Planets* **114**, E08S92 (2009).
14. A. C. Horleston *et al*., *Seism. Rec.* **2**, 88–99 (2022).
15. D. E. Gault, J. A. Wedekind, *Lunar Planet. Sci. Conf. Proc.* **3**, 3843–3875 (1978).
16. D. Elbeshausen, K. Wünnemann, G. S. Collins, *J. Geophys. Res. Planets* **118**, 2295–2309 (2013).
17. B. Ivanov *et al*., "New craters on Mars: Air shock wave traces," EGU General Assembly 2020, 4 to 8 May 2020, EGU2020-4212 (2020).
18. A. S. McEwen *et al*., *J. Geophys. Res. Planets* **112**, E05S02 (2007).
19. C. M. Dundas *et al*., *J. Geophys. Res. Planets* **126**, e2020JE006617 (2021).
20. K. L. Tanaka *et al*., Geologic Map of Mars: U.S. Geological Survey Scientific Investigations Map 3292 (USGS, 2014); https://doi.org/10.3133/sim3292.
21. P. Lesage, M. J. Heap, A. Kushnir, *J. Volcanol. Geotherm. Res.* **356**, 114–126 (2018).
22. C. Larmat, K. Onodera, R. Maguire, P. Lognonné, Modelling to resolve whether SEIS, the seismometer of the NASA Insight lander, has detected the formation of a 1.5m diameter crater which occurred about 40km away, Institut de Physique du Globe de Paris (IPGP) (2020); https://doi.org/10.18715/jgr_newcratermod_2020.
23. I. J. Daubar *et al*., *J. Geophys. Res. Planets* **125**, e2020JE006382 (2020).
24. InSight Mars SEIS Data Service, SEIS raw data, Insight Mission, IPGP, JPL, CNES, ETHZ, ICL, MPS, ISAE-Supaero, LPG, MFSC (2019); https://doi.org/10.18715/SEIS.INSIGHT.XB_2016.
25. P. Lognonné *et al*., *Nat. Geosci.* **13**, 213–220 (2020).
26. W. R. Walter, K. F. Priestley, in *Explosion Source Phenomenology*, S. R. Taylor, H. J. Patton, P. G. Richards, Eds. (American Geophysical Union, 1991), pp. 219–228.
27. S. R. Ford *et al*., "Toward an empirically-based parametric explosion spectral model," accession no. ADA568895 (Lawrence Livermore National Lab, 2011); https://apps.dtic.mil/sti/citations/ADA568895.
28. M. Böse *et al*., *Bull. Seismol. Soc. Am.* **111**, 3003–3015 (2021).
29. N. Wójcicka *et al*., *J. Geophys. Res. Planets* **125**, e2020JE006540 (2020).
30. A. Rajšić *et al*., *J. Geophys. Res. Planets* **126**, e2020JE006662 (2021).
31. N. A. Teanby, J. Wookey, *Phys. Earth Planet. Inter.* **186**, 70–80 (2011).
32. I. Daubar *et al*., *Space Sci. Rev.* **214**, 132 (2018).
33. J. D. Okeefe, T. J. Ahrens, *Lunar Planet. Sci. Conf. Proc.* **3**, 3357–3374 (1977).
34. I. V. Nemtchinov, V. V. Shuvalov, R. Greeley, *J. Geophys. Res.* **107**, 17-1–17-8 (2002).
35. S. Glasstone, P. J. Dolan, "The effects of nuclear weapons," ed. 3 (Tech. Rep. TID-28061, U.S. Department of Defense, U.S. Department of Energy, 1977); https://doi.org/10.2172/6852629.
36. P. Lognonné, B. Mosser, F. A. Dahlen, *Icarus* **110**, 180–195 (1994).
37. M. N. Toksöz, A. Ben-Menahem, *J. Geophys. Res.* **69**, 1639–1648 (1964).
38. D. G. Harkrider, C. A. Newton, E. A. Flinn, *Geophys. J. Int.* **36**, 191–225 (1974).
39. P. Lognonné, F. Karakostas, L. Rolland, Y. Nishikawa, *J. Acoust. Soc. Am.* **140**, 1447–1468 (2016).
40. K. Onodera, T. Kawamura, S. Tanaka, Y. Ishihara, T. Maeda, *J. Geophys. Res. Planets* **126**, e2020JE006406 (2021).
41. InSight Marsquake Service, Mars Seismic Catalogue, InSight Mission; V11 2022-07-01, ETHZ, IPGP, JPL, ICL, Univ. Bristol (2022); https://doi.org/10.12686/a17.
42. M. Böse *et al*., *Phys. Earth Planet. Inter.* **262**, 48–65 (2017).
43. J. F. Clinton *et al*., *Phys. Earth Planet. Inter.* **310**, 106595 (2021).
44. C. Durán *et al*., *Phys. Earth Planet. Inter.* **325**, 106851 (2022).
45. S. C. Stähler *et al*., *Science* **373**, 443–448 (2021).
46. A. Khan *et al*., *Science* **373**, 434–438 (2021).
47. A. Khan, P. A. Sossi, C. Liebske, A. Rivoldini, D. Giardini, *Earth Planet. Sci. Lett.* **578**, 117330 (2022).
48. M. Drilleau *et al*., *J. Geophys. Res. Planets* **127**, e2021JE007067 (2022).
49. M. C. Malin, K. S. Edgett, *J. Geophys. Res.* **106**, 23429–23570 (2001).
50. D. E. Smith *et al*., *J. Geophys. Res.* **106**, 23689–23722 (2001).

ACKNOWLEDGMENTS

Any use of trade, firm, or product names is for descriptive purposes only and does not imply endorsement by the U.S. Government. This is InSight contribution 221 and LA-UR-22-27122. We acknowledge NASA, CNES, partner agencies and institutions (UKSA, SSO, DLR, JPL, IPGP-CNRS, ETHZ, ICL, and MPS-MPG), and the operators of JPL, SISMOC, MSDS, IRIS-DMC, and PDS for providing SEED SEIS data. This research was carried out in part at the Jet Propulsion Laboratory, California Institute of Technology, under a contract with NASA. **Funding:** This work was funded by NASA-NNN12AA01C with subcontract JPL-1515835 (L.V.P., M.C.M., B.A.C., C.K., G.S., D.S., A.V., and A.W.); NASA-80NM0018D0004 (W.B.B., M.G., and M.Pa.) InSight PSP grant 80NSSC20K0971 (I.J.D.) and 80NSSC18K1626 (R.L); the MRO HiRISE project (C.M.D.); ETH Zurich through the ETH+ funding scheme (ETH+02 19-1: "Planet Mars") (J.C., D.G., S.C., S.C.S., C.D., N.D., A.K., D.K., and G.Z.); ETH research grant ETH-10 17-3 (S.C.S.); UK Space Agency grants ST/R002096/1, ST/V00638X/1, ST/T002026/1, ST/S001514/1, and ST/W002523/1 (A.H., C.C., N.A.T., G.S.C., N.W., and W.T.P.); the Australian Research Council (DP180100661 and FT210100063) (K.M. and A.R.); the French Space Agency CNES and ANR fund (ANR-19-CE31-0008-08) (P.L., T.K., M.F., Z.X., É.B., R.F.G., L.M., S.M., C.Pa., C.Pe., M.Pl., L.R., A.Sp., A.St., and M.D.); and the Center for Space and Earth Science of LANL (Student Fellow Project) (M.F., C.L., and E.R.). This study contributes to IdEx Université Paris Cite ANR-18-IDEX-0001 (P.L., T.K., M.F., Z.X., S.M., C.Pa., M.Pl., and M.D.). **Author contributions:** Lead of the CTX/imaging interpretation: L.V.P. Lead of the SEIS interpretation: P.L. Text contributions: B.F., I.J.D., G.S.C., J.C., L.V.P., P.L., S.C.S., T.K., and Z.X. Edits to the main text and supplementary materials: B.F., I.J.D., M.E.B., R.L., S.C., K.M., and S.C.S. Figure contributions: A.V., B.A.C., C.K., G.S., J.C., L.V.P., M.C.M., P.L., S.C., T.K., K.M., and M.F. Data services: C.Pa., C.Pe., and F.E. Geological interpretation: M.E.B., M.G., and M.C.M. Seismic analysis: A.H., C.C., C.D., C.Pe., D.K., É.B., G.Z., J.C., M.D., M.Pa., M.Pl., N.D., P.D., S.C., S.C.S., T.K., and W.T.P. Seismic interpretation: A.H., A.K., D.G., D.K., J.C., L.M., M.F., P.D., S.M., S.C.S., T.K., W.T.P., and Z.X. Image analysis: A.W., B.A.C., C.M.D., C.K., D.S., G.S., I.J.D., L.V.P., and M.C.M. Targeting orbital assets: A.W., C.D., D.S., G.S., I.J.D., and L.V.P. Seismic moment analysis: P.L., T.K., and Z.X. Impact model contribution and/or simulations: A.R., C.L., G.S.C., K.M., N.W., and R.L. Seismo-atmosphere coupling work: A.Sp., L.R., M.F., P.L., T.K., and Z.X. Seismic source modeling discussion: C.L., E.R., M.F., N.A.T., and P.L. Seismic efficiency analysis: A.St. and N.A.T. Search for atmospheric signals: A.St., P.L., and R.F.G. InSight mission management: W.B.B. and M.Pa. SEIS instrument development and management: P.L., D.G., W.T.P., and W.B.B. CTX/MARCI development: M.C.M. CTX/MARCI management: L.V.P. **Competing interests:** The authors declare that they have no competing interests. **Data and materials availability:** MRO data are available from the NASA-PDS repository. The InSight event catalog and waveform data are available from the IRIS-DMC, NASA-PDS, SEIS-InSight data portal, and IPGP data center.

SUPPLEMENTARY MATERIALS

science.org/doi/10.1126/science.abq7704
Materials and Methods
Figs. S1 to S10
Tables S1 and S2
References (*51–73*)

Submitted 29 April 2022; accepted 22 September 2022
10.1126/science.abq7704

Science

Largest recent impact craters on Mars: Orbital imaging and surface seismic co-investigation

L. V. PosiolovaP. LognonnéW. B. BanerdtJ. ClintonG. S. CollinsT. KawamuraS. CeylanI. J. DaubarB. FernandoM. FromentD. GiardiniM. C. MalinK. Miljkovi#S. C. StählerZ. XuM. E. BanksÉ. BeuclerB. A. CantorC. CharalambousN. DahmenP. DavisM. DrilleauC. M. DundasC. DuránF. EuchnerR. F. GarciaM. GolombekA. HorlestonC. KeeganA. KhanD. KimC. LarmatR. LorenzL. MargerinS. MeninaM. PanningC. PardoC. PerrinW. T. PikeM. PlasmanA. Rajši#L. RollandE. RougierG. SpethA. SpigaA. StottD. SuskoN. A. TeanbyA. ValehA. WerynskiN. WójcickaG. Zenhäusern

Science, 378 (6618), • DOI: 10.1126/science.abq7704

An insightful impact

On 24 December 2021, the seismometer for the InSight mission on Mars detected a large seismic event with a distinct signature. Posiolova *et al*. discovered that the event was caused by a meteor impact on the surface of Mars, which was confirmed by satellite observations of a newly formed 150-kilometer crater. The surface nature and size of the impact allowed Kim *et al*. to detect surface waves from the event, which have yet to be observed on Mars. These surface waves help to untangle the structure of the Martian crust, which has various amounts of volcanic and sedimentary rock, along with subsurface ice, in different regions of the planet (see the Perspective by Yang and Chen). The characteristics of the impact itself are important because they provide a seismic fingerprint of an impact event that is different from the marsquakes observed so far. —BG